Nuclear Inst, and Methods in Physics Research B 429 (2018) 27–33

Contents lists available at ScienceDirect

Nuclear Inst. and Methods in Physics Research B

journal homepage: www.elsevier.com/locate/nimb

# Neutron energy spectrum measurement using an NE213 scintillator at CHARM

Tsuyoshi Kajimoto[a,*], Toshiya Sanami[b], Noriaki Nakao[c], Robert Froeschl[d], Stefan Roesler[d], Elpida Iliopoulou[d,e], Angelo Infantino[d], Markus Brugger[d], Eunji Lee[f], Nobuhiro Shigyo[f], Masayuki Hagiwara[b], Hiroshi Yashima[g], Hirohito Yamazaki[b], Kenichi Tanaka[a], Satoru Endo[a]

[a] Hiroshima University, 1-4-1, Kagamiyama, Higashi-Hiroshima 739-8527, Japan
[b] High Energy Accelerator Research Organization, Oho, Tsukuba 305-0801, Japan
[c] Shimizu Corporation, 3-4-17 Etchujima, Koto-ku, Tokyo 135-8530, Japan
[d] CERN, 1211 Geneva 23, Switzerland
[e] Aristotle University of Thessaloniki, Thessaloniki 54124, Greece
[f] Kyushu University, Motooka, Nishi-ku, Fukuoka 819-0395, Japan
[g] Research Reactor Institute, Kyoto University, 2-1010 Asashiro-nishi, Kumatori, Sennan, Osaka 590-0494, Japan

ARTICLE INFO

*Keywords:*
CHARM
Neutron energy spectrum
Fluence
NE213 scintillator
Unfolding

ABSTRACT

To establish a methodology for neutron spectrum measurement at the CERN High energy AcceleRator Mixed field facility (CHARM), neutron spectra were measured using an NE213 scintillator on top of the CHARM roof shielding where is the CERN Shielding Benchmark Facility (CSBF). The spectra were derived as fluences into the scintillator by the unfolding method using an iterative Bayesian algorithm. The methodology was verified based on the agreement of two spectra measured for different positions and directions of incident neutrons by changing the detector orientation. Since the spectra on the roof-top were obtained within a reasonable beam-time, this methodology is suitable for measuring the spectrum when there is less shielding material. Thus, experimental data for neutron transition can be obtained as a function of shielding thickness using this facility.

## 1. Introduction

The energy spectra and attenuation lengths of secondary neutrons, which are generated through hadronic cascade reactions in a target, in a beam line tunnel, and shielding structure are of primary importance for the shielding design of high-energy and high-power hadron accelerators. These quantities have recently been estimated using Monte Carlo codes such as FLUKA [1,2], GEANT4 [3], MARS [4], and PHITS [5], which are based on theoretical models and parameters for not only a simple bulk geometry but also complex maze structures. For verification and validation of these codes, results of the codes should be examined through the comparison with experimental data obtained for an actual, well-defined geometry as well as models and parameters.

To date, several experiments have been performed to obtain the energy spectra and attenuation of secondary neutrons at high-energy accelerator facilities. Neutron energy spectra from several target materials have been measured for a 40 GeV/c mixed beams of protons and pions at the CERN-European Union High-Energy Reference Field (CERF) using Bonner spheres [6] and for 120 GeV protons at the MTest of the Fermi National Accelerator Laboratory (FNAL) using time-of-flight method with an NE213 scintillator [7–9]. Neutron energy spectra behind shielding have been measured at the CERF using Bonner spheres [10,11] and an NE213 scintillator [12] with the unfolding technique, and at the FNAL pbar using 120 GeV protons with Bonner spheres [13]. According to these experiments, there are notable differences between calculation and experimental results. To explore the reasons for these differences experimentally, a facility is needed to measure neutron energy spectra and attenuation under various-conditions, such as different target and shielding materials, and its thicknesses, with various types of neutron detectors.

The CERN High energy AcceleRator Mixed field facility (CHARM) has been constructed to evaluate the radiation hardness of devices and equipment subjected to secondary-particle fields from high-energy hadron cascade reactions [14,15]. It receives a proton beam with momentum of 24 GeV/c and adjustable intensity. The facility, consists of a large irradiation space inside its shielding enclosure, a remote-controlled target holder, four movable shielding walls, a maze structure for access to the irradiation space, and replaceable roof shielding blocks

* Corresponding author.
*E-mail address:* kajimoto@hiroshima-u.ac.jp (T. Kajimoto).

https://doi.org/10.1016/j.nimb.2018.05.024
Received 24 August 2017; Received in revised form 27 March 2018; Accepted 14 May 2018
Available online 22 May 2018

that are more than 3 m thick. Thus, this facility is suitable to obtain systematic data for neutron energy spectra and attenuation under various conditions.

In this study, we measured neutron spectra using an NE213 scintillator on top of the CHARM roof shielding where was the CERN Shielding Benchmark Facility (CSBF), to establish a methodology for neutron energy spectrum measurement at this facility. The top of the roof is located 6.75 m laterally above the target with a shielding structure. This corresponds to the maximum shielding condition for 90 degrees vertically to the beam axis. If neutron spectrum can be obtained under this condition within a reasonable beam-time, then the spectrum can be obtained when there is less shielding material, owing to sufficient beam intensity. The thickness of removable shield was estimated to be 170 cm for concrete under the same detector position and beam intensity of this measurement. This would mean that experimental data for neutron transition could be obtained as a function of the shielding thickness using this facility.

We chose an NE213 scintillator as the neutron detector since it provides a neutron spectrum in the energy range from several to a few hundred MeV. The unfolding technique was applied to deduce the neutron energy spectrum behind a shielding wall, where the time-of-flight technique was not applicable. Bonner spheres are another type of detector that could be used, as it covers the energy range from eV to MeV. There are overlaps in the energy range of both spectra. However, the spectrum obtained with an NE213 scintillator provides a more detailed shape in the energy range in which the physical models treat nuclear reactions in the calculation codes. Furthermore, higher energy neutrons are sources of lower energy neutrons, so the detailed spectrum in the higher energy range is important for validating the calculation results given by the codes.

## 2. Structure of CHARM from the viewpoint of a shielding experiment

CHARM was constructed in the Proton Synchrotron (PS) East Area hall. Fig. 1 shows a plan view of CHARM at beam line height, 125 cm above the floor. The target is located in the irradiation room, which has an approximately $5 \times 7 \times 3.6\ m^3$ (L × W × H) area enclosed by shielding walls made of marble, concrete, and iron. The 24 GeV/c proton beam bombards the target to produce a radiation field of secondary particles. The space around the target is used for irradiation of devices and equipment that are to be tested for radiation hardness. To control the intensity of the radiation field, the target holder with three targets and four plates of movable shield walls are installed in the irradiation space. A beam dump consisting of 8-m-thick iron is located 7.2 m downstream

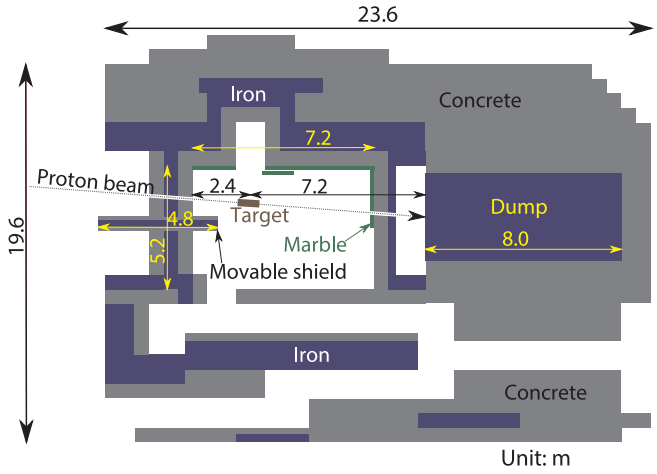


**Fig. 1.** Plan view of CHARM at beam-line height. The movable shield is set in the off-position in this experiment.

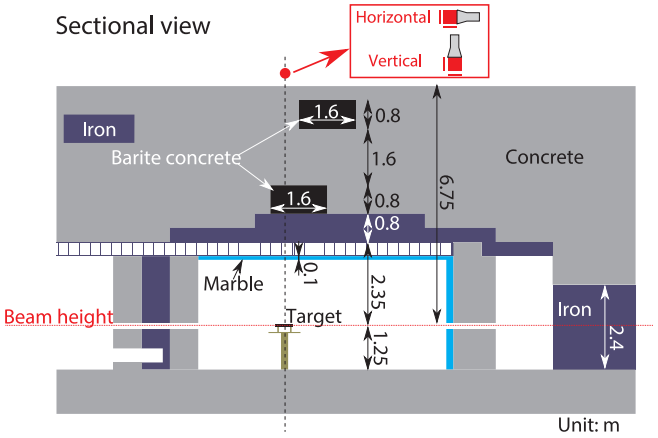


**Fig. 2.** Sectional view of CHARM on vertical plane of beam line. In this experiment, an NE213 scintillator was set on top of the CSBF that is integrated into the concrete shielding structure of CHARM.

from the target. A wall of concrete and iron with a beam hole is placed in front of the beam dump to avoid particle reflections. This arrangement enables measurement of the secondary particles directly from the target at an angle perpendicular to the primary beam.

The access corridor to the irradiation space has the maze structure to reduce the radiation leakage dose. The structure is suitable for collecting experimental data on the propagation of low-energy neutrons. These data should be useful as a reference for benchmarking Monte Carlo codes, since the radiation field at the entrance of the maze should be well known because of the simple target, the simple room structure, and less reflection from the beam dump.

Fig. 2 shows a sectional view of CHARM on vertical plane along the beam-line. The CSBF is integrated into the roof shielding of CHARM [15]. The roof shielding above the target consists of a 40-cm-thick iron block, an additional 40-cm-thick iron block, and concrete blocks. By removing or replacing the additional iron and concrete blocks, neutron attenuation data can be obtained for quite simple shielding structures consisting of 40-cm-thick iron and material with a thickness between 0 and 3.6 m.

The 24 GeV/c primary proton beam from the PS is transported through the air to the target. The intensity of the beam is $5 \times 10^{11}$ protons per spill. Each spill has typically a duration of 350 ms. The spills belong to a super-cycle of the PS, and are supplied to not only CHARM but also other facilities. Protons are injected into CHARM at a rated of up to $6.7 \times 10^{10}$ protons/s. The number of protons in a spill can be reduced down to 10% or less to mitigate the count rate of a secondary particle detector for an experiment.

The beam parameters are monitored using several devices installed along the beam-line. The beam intensity is recorded spill by spill using a secondary emission chamber (SEC) [16]. The SEC is installed right after the extraction port from the PS. The number of protons incident on the target, can be deduced by multiplying the count of the SEC by a calibration factor of $1.87 \times 10^7$ (protons/count) [17]. The beam position and size are monitored in real time by four beam profile monitors (BPMs) consisting of 40-channel metal foil detectors. The BPMs are placed on the beam-line more than 8 m upstream of the target.

In summary, the facility has the potential to allow us to measure the experimental data of secondary particles originating from 24 GeV/c protons for both direct exposure and attenuation by concrete with thickness of up to 3.6 m.

## 3. Experiment

### 3.1. Experimental setup

The neutron detector, a $\Phi 12.7 \times 12.7\ cm^3$ NE213 scintillator

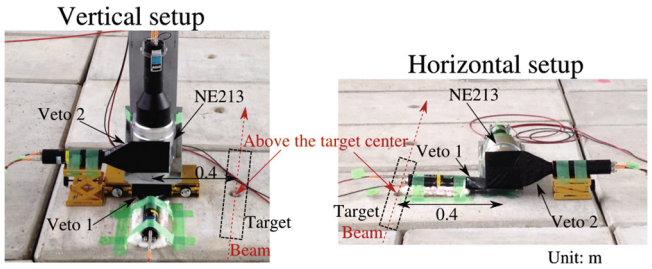


**Fig. 3.** Photographs of the vertical and horizontal setups. The NE213 detector was set at two different positions as the the flat or circular surface facing the concrete.

coupled with a photomultiplier tube (R1250, Hamamatsu), was set on top of the concrete shielding. The thickness and material of the shields from the target to the top were 10-cm-thick marble, 80-cm-thick iron and 360-cm-thick concrete (80-cm-thick barite concrete and 280-cm-thick normal concrete). Fig. 3 shows the two different detector setups that were used: a "vertical setup" with the detector facing the concrete surface toward the target and a "horizontal setup" with the detector parallel to the primary proton beam, facing the upstream direction. These two setups were used to confirm the effect of detector orientation on the measured neutron spectrum because the detector sensitivity depends on the position and direction of incident neutrons. For both setups, the detector was set 40 cm away from the position just above the target center as shown in Fig. 3. The vertical distances between the target center and the center of the NE213 scintillator were 694 and 688 cm for the vertical and horizontal setups, respectively. As veto detectors, two NE102A plastic scintillators were set at the bottom of the detector (Veto 1) and beam upstream to the detector (Veto 2). The Veto 1 and 2 detectors had dimensions of $15\times15\times0.6\,cm^3$ and $15\times15\times0.3\,cm^3$, respectively.

The 24 GeV/c protons were bombarded onto a $\Phi8\times50\,cm^3$ copper target (density: 8.96 g/cm$^3$). For every super-cycle containing 30–47 spills, 1–5 spills were assigned to CHARM. The number of protons monitored by the SEC was $3–4\times10^{11}$ protons/spill during this experiment. The beam was centered with diameters of 1.6 cm (horizontal) and 1.4 cm (vertical) full width at half maximum, measured by using the BPM placed near the target. The energy deposition of protons penetrating the target was calculated with SPAR [18] to be $7.9\times10^2$ MeV. The transmission rate for protons impinging on the target was estimated to be $1.1\times10^{-4}$ by using hadronic total cross sections calculated with systematics by Niita et al. [19]. Thus, most protons in the beam interacted with the target nuclei.

Sufficient count statistics were acquired at the NE213 detector in a measuring time of less than 20 h. The counts originating in the proton beam were $6\times10^2$–$7\times10^2$ counts/spill. The numbers of spills were 4679 and 5388 for measurements in the vertical and horizontal setups, respectively. The measuring time is expected to be reduced to a few hours when there is less shielding material. Thus, the shielding experiment with this detector can be performed at CHARM with a reasonable machine time.

### 3.2. Data acquisition system

Fig. 4 shows a time chart of signals from the detectors and the accelerator. The signal from the accelerator, called the pre-trigger, is delivered prior to the beam arrival at the target. The data acquisition system was activated during 700 ms from the pre-trigger (hereafter, beam gate). The length of the beam gate signal was sufficient to cover the actual beam spill length.

During the beam gate shown in Fig. 4, the integrated value of the signal was recorded together with the elapsed time from the start of data acquisition. The elapsed time was calculated as the time difference between the pre-trigger and the NE213 detector signal event by event.

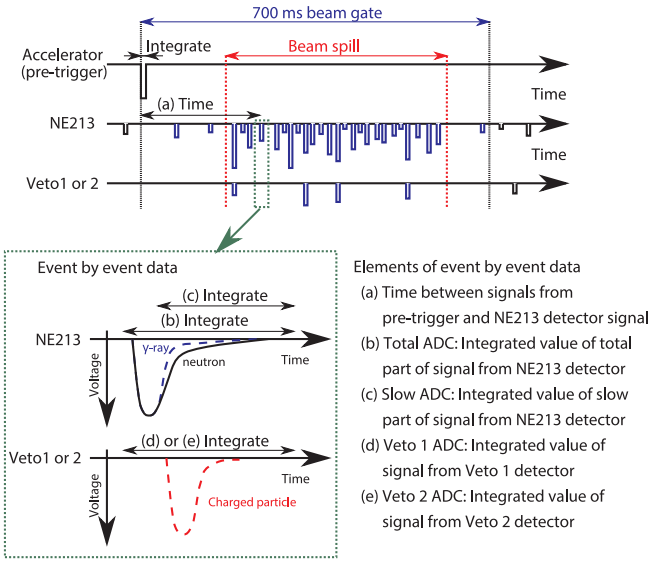


**Fig. 4.** Time chart of signals from the detectors and the accelerator, together with elements of event-by-event data.

To discriminate neutrons from $\gamma$-rays, two integrated values of the signal from the NE213 detector were acquired with two gates covering the total and slow parts of the signal. The integrated values of the veto detector signals were obtained by using the total gate to distinguish charged particles from uncharged particles. The integrated values were recorded with analog-to-digital converters (ADCs; A3200, Nikiglass Co., Ltd.). In summary, the event-by-event data consists of the time between the pre-trigger and the NE213 detector signal, the ADC values for the total and slow parts of the signal from the NE213 detector, and the ADC values for the signals of each veto detector.

Fig. 5 shows a schematic diagram of electronics circuit. The electronics circuit consisted of NIM and VME modules. The pre-trigger was fed to a gate generator 1 (G.G.1). G.G.1 generated the ADC input and gate for the pre-trigger to obtain the elapsed time. Moreover, the signal from the G.G.1 was fed to a gate generator 2 (G.G.2) which extended the signal width to 700 ms (beam gate). The signal from the NE213 detector was divided into two signals once again. One of the signals was divided in two signals, and the both signals were connected to the inputs of the ADCs. The other signal was connected to a constant fraction discriminator (CFD) to generate an NIM signal. The coincidence between the signal from the CFD and the beam gate was performed at a coincidence module (COIN). The output signals of the COIN were fed to a scaler and two gate generators (G.G.3 and G.G.4). The count in the scaler was used to correct for the counting loss of events occurring in the conversion process of ADCs. G.G.3 and G.G.4 were used to make the ADC gates of the NE213, Veto 1, and Veto 2 detectors. The gate lengths

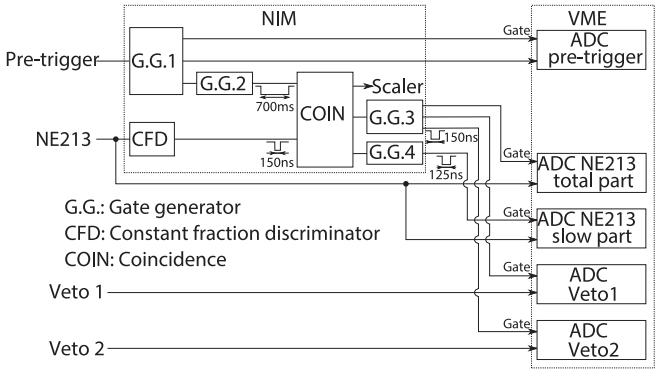


**Fig. 5.** Schematic diagram of the electronics circuit.

of the total and slow parts of the signal from the NE213 detector were set to be 150 and 125 ns, respectively. The gate of the total part was earlier than that of the slow part by 25 ns. The signals from each veto detector were directly connected to the inputs of the ADCs.

## 4. Data analysis

### 4.1. Spectrum unfolding

The neutron energy spectra were obtained as energy-dependent neutron fluences into the scintillator. The neutron fluence $\frac{dY(E)}{dE}$ was derived from

$$\frac{dY(E)}{dE} = \frac{S(E)}{B\,A\,\Delta E}, \tag{1}$$

where $\Delta E$ is the energy bin width of the spectrum, $B$ is the number of protons derived from the measured counts of the SEC, and $A$ is the effective detector surface area derived from track length estimation. Finally, $S(E)$ is the incident neutron spectrum on the NE213 scintillator with energy $E$, and was derived using the unfolding method.

In the unfolding process, we used the iterative Bayesian algorithm [20] in the RooUnfold package [21]. The relation between the incident neutron spectrum with the energy $E$, $S(E_i)$ at $i$th energy bin, and neutron light output spectrum with the light output $L$, $N(L_j)$ at $j$th light output bin, is expressed as

$$S(E_i) = \sum_{j=1} N(L_j)\,P(E_i|L_j), \tag{2}$$

where $N(L_j)$ was obtained by analyzing event-by-event data. The conditional probability $P(E_i|L_j)$ is expressed as

$$P(E_i|L_j) = \frac{P(L_j|E_i)\,P(E_i)}{\sum_{l=1}^{n_E} P(L_j|E_l)\,P(E_l)}, \tag{3}$$

where $P(E_i)$ is the probability of the incident neutron number in $i$th energy bin to that in all energy bins, and $n_E$ is the number of energy bins. The detector response is indicated as the conditional probability $P(L_j|E_i)$ in cases to obtain a light output $L_j$ from the NE213 detector when neutrons with mono energy $E_i$ enter in the NE213 detector, and was obtained by simulation. In the unfolding method, $S(E)$ was derived by giving an initial distribution to $P(E)$.

### 4.2. Neutron light output spectrum

The neutron light output spectrum was deduced by event selection and light output calibration. Events originating in the beam and identified neutrons were extracted from the event-by-event data.

Events originating in the beam were discriminated with a scatter plot showing the counts for each spill as a function of the time difference between the pre-trigger and the NE213 detector signal, as shown in Fig. 6. Beam on and off target periods distinguished by the count difference. The events between 180 and 640 ms shown in Fig. 6 were selected as beam events.

Neutron events were obtained by selection of uncharged particle events and pulse shape discrimination (PSD). Charged and uncharged particle events were distinguished using the scatter plots of total ADC versus Veto 1 and total ADC versus Veto 2, as shown in Fig. 7. The band corresponding to proton events can be observed in the scatter plots of total ADC versus Veto 1. PSD was performed with a scatter plot of total versus slow ADCs as shown in Fig. 8. Because the neutron and $\gamma$-ray events overlap with one another in the low total ADC region, the discrimination threshold of the total ADC was chosen as 227 ch, which corresponds to 3.1 MeVee (MeV electron equivalent) in the vertical setup and 3.0 MeVee in the horizontal setup. The loss of neutron events due to the overlap was less than 5% at the threshold.

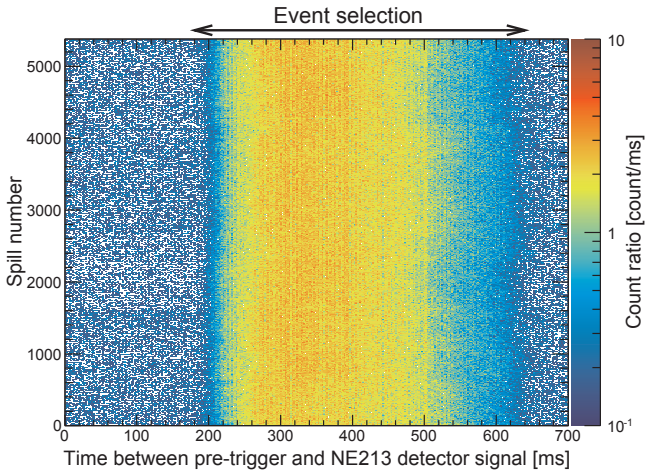


**Fig. 6.** Scatter plot of the counts for each spill as a function of the time difference between the pre-trigger and the NE213 detector signal, in the horizontal setup measurement. Events in the period between 180 and 640 ms were selected as beam events.

The values of the total ADC were converted to the light output values (in MeVee). In the light output region below 5 MeVee, the calibration points were obtained from Compton edges of $\gamma$-rays from check sources. The check sources and the $\gamma$-ray energy were 0.662 MeV for $^{137}$Cs, 1.17 and 1.33 MeV for $^{60}$Co, 1.28 MeV for $^{22}$Na, and 4.43 MeV for $^{241}$AmBe. Cosmic-ray muons were measured in natural background measurement. Since the events by muons penetrating the NE213 detector formed a broad peak, the peak was used as a calibration point at which the light output was 20.5 MeVee [22]. The point around 100 MeVee was obtained from the maximum energy deposition of protons shown in Fig. 7. The protons were produced in the concrete shield under the NE213 detector not directly from the target.

Fig. 9 shows the neutron light output spectrum. The spectrum of the events during the beam-off period is also shown to investigate the contributions from the loss in the beam event extraction and from the natural background. The losses are observed because the shapes of both spectra are similar. Furthermore, the similarities between the shapes mean that the contribution from the natural background is negligibly small compared with the loss in the beam event extraction. Since the loss was less than 0.1% compared to the beam on target period, these contributions were ignored.

The neutron light output spectrum was multiplied by the ratio of the number of recorded events to the scaler counts due to correct for the counting loss of events occurring in the conversion process of the ADC. The ratios were 1.005 and 1.003 in the vertical and horizontal setup measurements, respectively.

### 4.3. Detector response and effective detector surface area

The detector responses and the effective detector surface area were calculated using the SCINFUL-QMD code [23,24], taking into account the position and direction of the incident neutrons. Fig. 10 shows the geometries used for the calculations. Source neutrons with uniform energy distribution up to 300 MeV were isotropically and uniformly generated inside a circle with a diameter of 10 m. A scoring region with the same shape and size as the NE213 scintillator used in this experiment was set above the center of this circle.

The light output and straight-line length from the incident point to the detector wall were calculated when the neutron entered the scoring region. The light output was smeared with its resolution. The resolution was determined using the experimental data for the Compton edges of $\gamma$-rays for $^{137}$Cs, $^{60}$Co, $^{22}$Na, and $^{241}$AmBe. The light output resolution above 5 MeVee was determined to be about 3.5%.

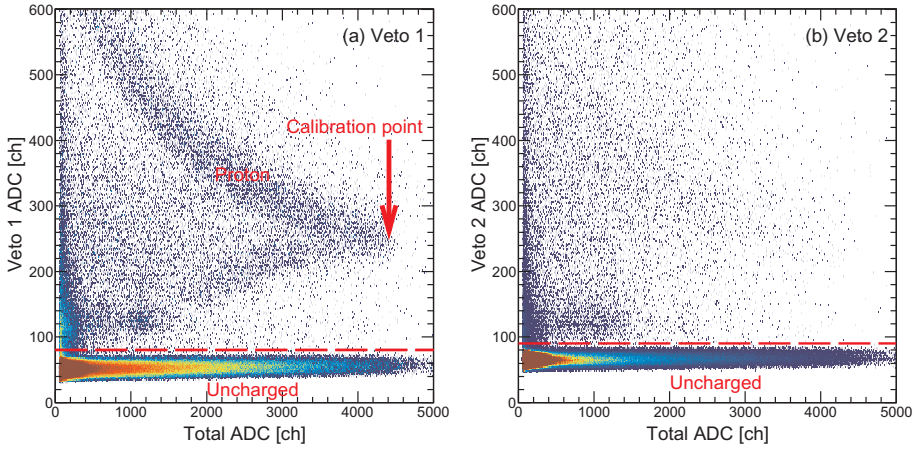


**Fig. 7.** Scatter plots of (a) total ADC versus Veto 1, and (b) total ADC versus Veto 2, in the vertical setup. The band corresponding to the proton events can be observed in the scatter plot for total versus Veto 1 ADCs.

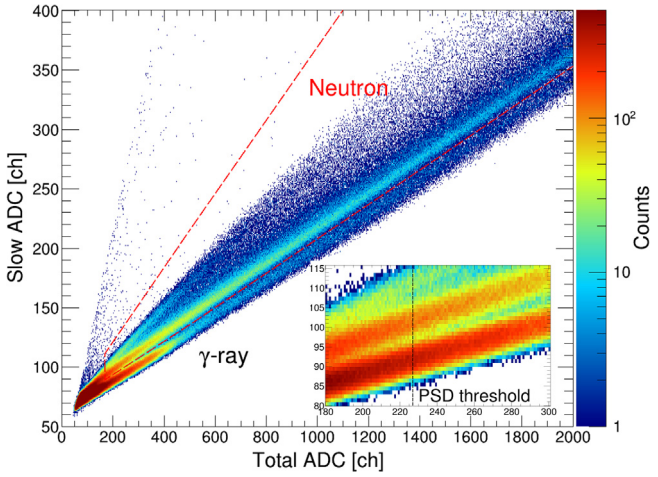


**Fig. 8.** Scatter plot of total versus slow ADCs in the vertical setup. Events in the region surrounded by broken lines were extracted as those of neutrons. The discrimination threshold of the total ADC was chosen as 227 ch.

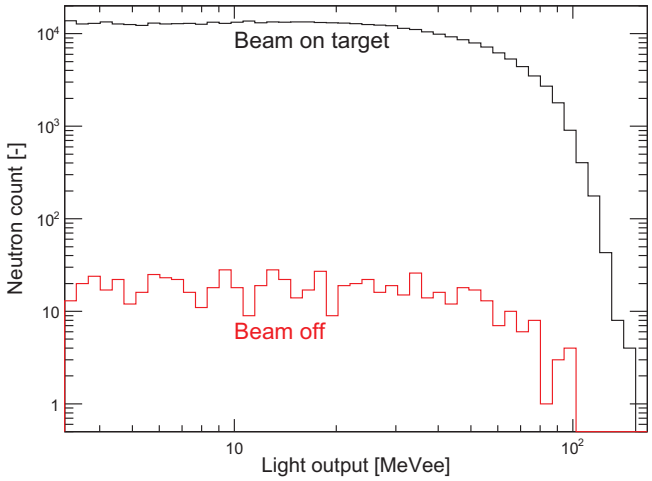


**Fig. 9.** Neutron light output spectrum for the horizontal setup measurement. The spectrum of the events during the beam-off period is also shown to investigate the contributions from the loss in the beam event extraction and from the natural background.

The detector responses were calculated by scoring the incident neutron energy and the light output. The effective detector surface area $A$ was derived from the following equation [25]:

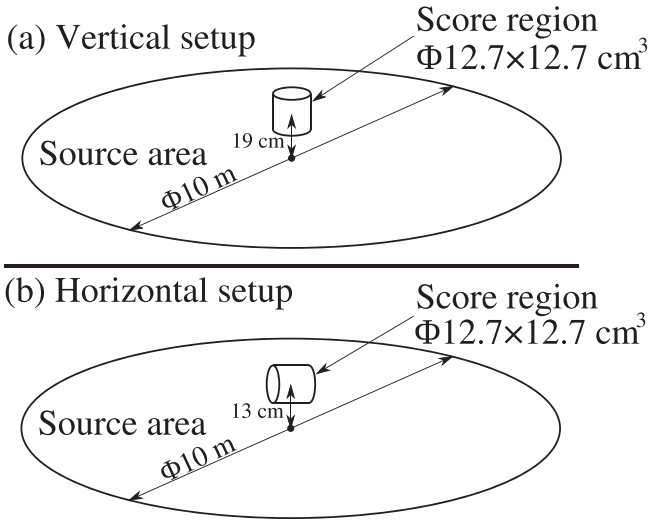


**Fig. 10.** Geometries of the (a) vertical and (b) horizontal setups to calculate the detector responses and the effective detector surface area. The SCINFUL-QMD code was used for the calculations.

$$A = \frac{V}{l_{av}}, \tag{4}$$

where $V$ is the volume of the NE213 scintillator and $l_{av}$ is the track length, which is the average of the straight-line lengths from the incident point to the detector wall. The track length corresponds to an index of the dependence on the position and direction distributions, and is estimated to be 7.42 and 5.80 cm for the vertical and horizontal setups, respectively.

## 5. Results and discussion

Fig. 11 shows the neutron energy spectra for the vertical and horizontal setups, as well as the ratio of the spectra for horizontal setup to vertical setup. The edge of the lowest energy bin of the measured spectra was determined by the threshold of the PSD. The measured spectra have only uncertainty originating in the unfolding [21]. The uncertainties of each bin are less than 8%. A broad peak in the energy range between 20 and 30 MeV is significantly observed in both spectra. The broad peak component was formed during neutron transport in the iron shield placed above the target due to a depression of the total cross section, and remained during the neutron transmission through the concrete.

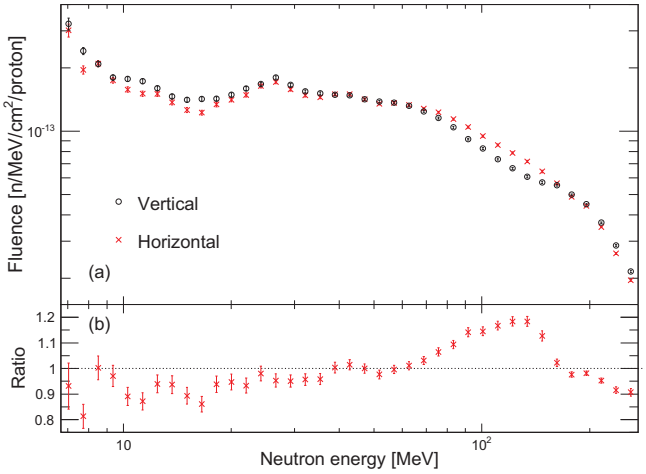


**Fig. 11.** (a) Measured neutron energy spectra. The energy range of the spectra is from 6.7 to 300.0 MeV. (b) Ratio of the spectra for horizontal setup to vertical setup.

In spite of the difference for the setups for the NE213 scintillator, the spectra are in good agreement with each other within the ratio difference less than 19%. The agreement is especially good in the energy range between 20 and 80 MeV. The integral values of the spectra in the energy range between 6.7 and 300 MeV were $2.11 \times 10^{-10}$ and $2.15 \times 10^{-10}$ (n/cm$^2$/proton) for the vertical and horizontal setups, respectively. These integral values are in good agreement with each other within the ratio difference less than 2%. The difference of integral values is consistent with the difference of the ratio of the inverse square of the distances between the target and the NE213 detector for the vertical and horizontal setups. These agreements indicate that the methodology of the calculations worked properly for detector responses and effective area. However, calculating the detector responses and the effective area with a three-dimensional particle transport Monte Carlo code will be required for more complex conditions, such as a detector surrounded by concrete walls.

The feasibility of the measurement using this facility with the NE213 detector is discussed for less shielding materials and using different targets. In this experiment, the count rate was less than $3 \times 10^3$ cps. The NE213 detector accepts count rates up to $10^5$ cps. The transmission rate $T$ is estimated as

$$T = \exp\left(-\frac{\rho}{\lambda} t\right), \tag{5}$$

where $\rho$ is the density of the shielding material (2.4 g/cm$^3$ for normal concrete and 3.35 g/cm$^3$ for barite concrete) [17], $\lambda$ is the attenuation length (120 g/cm$^2$ for normal concrete and 124 g/cm$^2$ for barite concrete) [26], and $t$ is the thickness of the shielding material. The half-value thickness and tenth-value thickness of normal concrete are 35 and 115 cm, respectively. With the same beam intensity as in this experiment, a measurement with current apparatus is feasible for the removal of 170 cm normal concrete, i.e. down to 80 cm thickness of iron and 190 cm thickness of concrete, respectively. Since the yield for the aluminum target is about 2.5 times less than for the copper target [15], the count rate of the aluminum target is estimated to be $10^3$ cps. Removing 220 cm thickness of normal concrete is thus acceptable for the aluminum target. A reduction of the beam intensity would be necessary to remove more shields. In order to remove the concrete shield entirely, the beam intensity would be reduced to about 1% of the current beam intensity for the copper target, and to about 4% for the aluminum target.

## 6. Summary

The neutron energy spectra were measured by using an NE213 detector on the roof top of CHARM. The NE213 detector was set in vertical and horizontal setups. The neutron energy spectra were derived from the unfolding method using an iterative Bayesian algorithm. The detector responses were calculated with the SCINFUL-QMD code, by taking into account the positions and directions of the incident neutrons. The neutron energy spectra were obtained as the fluences into the scintillator by dividing the energy spectra by the effective detector surface area, which was derived via track length estimation in the detector response calculation. Since the shapes of neutron energy spectra were in good agreement with each other, the measurement method was experimentally confirmed to be reasonable. It was also found that the measured spectrum had a broad peak at 20–30 MeV.

In future research, the detector response and the effective detector surface area should be investigated under more complex geometry, for various position and direction distributions of incident neutrons impinging on the detector. When the detector is placed on a flat open surface, the contribution due to the neutron distributions is expected to be small. However, this contribution may become more significant for measurements at a location surrounded with shielding or in a maze structure. Although there is a difficulty to determine the distributions, experimentally, the distributions could be obtained by the calculation by three dimensional Monte Carlo simulation codes. This will be the next step of this study.

The present method with the NE213 detector at CHARM is quite effective for measuring the neutron energy spectrum and attenuation in shielding. Further shielding experiments are desired to obtain the systematic data set and shielding properly. Comparisons between measured and calculated values will be useful for improvement and validation of empirical formulas and simulation codes.

## Acknowledgement

The authors thank the operation team of CHARM for their generous support of the experiment.

## References

[1] T. Böhlen, F. Cerutti, M. Chin, et al., The fluka code: developments and challenges for high energy and medical applications, Nucl. Data Sheets 120 (2014) 211–214.
[2] Fassò A, Ferrari A, Ranft J. et al., FLUKA: a multi-particle transport code, Tech. Rep. CERN-2005-10; 2005. INFN/TC-05/11, SLAC-R-773.
[3] S. Agostinelli, J. Allison, K. Amako, et al., Geant4a simulation toolkit, Nucl. Instrum. Methods Phys. Res., Sect. A 506 (3) (2003) 250–303.
[4] N.V. Mokhov, S.I. Striganov, Mars15 overview, AIP Conf. Proc. 896 (1) (2007) 50–60.
[5] T. Sato, K. Niita, N. Matsuda, et al., Particle and heavy ion transport code system, PHITS, version 2.52, J. Nucl. Sci. Technol. 50 (9) (2013) 913–923.
[6] S. Agosteo, C. Birattari, E. Dimovasili, et al., Neutron production from 40 GeV/c mixed proton/pion beam on copper, silver and lead targets in the angular range 30–135°, Nucl. Instrum. Methods Phys. Res., Sect. B 29 (1) (2005) 24–34.
[7] Y. Iwamoto, T. Sanami, T. Kajimoto, et al., Measurement of thick target neutron energy spectra at 15° and 90° bombarded with 120-GeV protons, Prog. Nucl. Sci. Technol. 3 (2012) 65–68.
[8] T. Sanami, Y. Iwamoto, T. Kajimoto, et al., Methodology for the neutron time of flight measurement of 120-GeV proton-induced reactions on a thick copper target, Nucl. Instrum. Methods Phys. Res., Sect. B 274 (2012) 26–35.
[9] T. Kajimoto, N. Shigyo, T. Sanami, et al., Measurements and parameterization of neutron energy spectra from targets bombarded with 120 GeV protons, Nucl. Instrum. Methods Phys. Res., Sect. B 337 (2014) 68–77.
[10] S. Agosteo, C. Birattari, A.F. Para, et al., Neutron measurements around a beam dump bombarded by high energy protons and lead ions, Nucl. Instrum. Methods Phys. Res., Sect. A 459 (12) (2001) 58–65.
[11] S. Agosteo, F. Pozzi, M. Silari, et al., Attenuation in iron of neutrons produced by 120 GeV/c positive hadrons on a thick copper target, Nucl. Instrum. Methods Phys. Res., Sect. B 312 (2013) 36–41.
[12] N. Nakao, S. Taniguchi, S. Roesler, et al., Measurement and calculation of high-energy neutron spectra behind shielding at the CERF 120 GeV/c hadron beam facility, Nucl. Instrum. Methods Phys. Res., Sect. B 266 (1) (2008) 93–106.
[13] M. Hagiwara, T. Sanami, Y. Iwamoto, et al., Shielding experiments at high energy accelerators of Fermilab (iii): neutron spectrum measurements in intense pulsed

neutron fields of the 120-GeV proton facility using a current bonner sphere technique, Prog. Nucl. Sci. Technol. 1 (2011) 52–56.
[14] Froeschl R. Radiation Protection Assessment of the Proton Irradiation facility and the CHARM facility in the East Area, CERN-RP-2014-008-406 REPORTS-TN, EDMS 1355933; 2014.
[15] R. Froeschl, M. Brugger, S. Roesler, The CERN high energy accelerator mixed field (CHARM) facility in the CERN PS east experimental area, Proc. Shielding Aspects Accel. Targets Irradiation Facil. SATIF 12 (2015) 14–25.
[16] Agoritsas V. Secondary emission chambers for monitoring the cps ejected beams, CERN-MPS-Int-CO-68-9; 1968.
[17] E. Iliopoulou, P. Bamidis, M. Brugger, et al., Measurements and FLUKA simulations of bismuth and aluminium activation at the CERN Shielding Benchmark Facility (CSBF), Nucl. Instrum. Methods A 885 (2018) 79–85.
[18] T.W. Armstrong, K.C. Chandler, A fortran program for computing stopping powers and ranges for muons, charged pions, protons, and heavy ions, ORNL-4869, Oak Ridge National Laboratory (1973).
[19] K. Niita, H. Takada, S. Meigo, et al., High-energy particle transport code NMTC/JAM, Nucl. Instrum. Methods Phys. Res., Sect. B 184 (3) (2001) 406–420.
[20] G. D'Agostini, A multidimensional unfolding method based on Bayes theorem, Nucl. Instrum. Methods Phys. Res., Sect. A 362 (2) (1995) 487–498.
[21] T. Adye, Unfolding algorithms and tests using RooUnfold, Proceedings of the PHYSTAT 2011 workshop on statistical issues related to discovery claims in search experiments and unfolding, 2011, pp. 313–318.
[22] T. Kajimoto, K. Tanaka, S. Endo, Light output due to cosmic-ray muons for an EJ301 scintillator of 12.7 cm in diameter and length, Nucl. Instrum. Methods A (2018) 53–57.
[23] D. Satoh, S. Kunieda, Y. Iwamoto, et al., Development of SCINFUL-QMD code to calculate the neutron detection efficiencies for liquid organic scintillator up to 3 GeV, J. Nucl. Sci. Technol. 39 (sup2) (2002) 657–660.
[24] T. Kajimoto, N. Shigyo, T. Sanami, et al., Measurement of absolute response functions and detection efficiencies of an NE213 scintillator up to 600 MeV, Nucl. Instrum. Methods Phys. Res., Sect. A 665 (2011) 80–89.
[25] L. Papiez, J.J. Battista, Radiance and particle fluence, Phys. Med. Biol. 39 (6) (1994) 1053–1062.
[26] K. Liu, G.R. Stevenson, R.H. Thomas, et al., Variance and regression analyses of Moyer model parameter data and their variation with primary proton energy, Health Phys. 46 (1984) 674–681.